**Thermal Conductivity/Diffusivity of SiC-Mullite and SiC-SiC Composites**

by

Laura M. Russell

Thesis submitted to the Faculty of the

Virginia Polytechnic Institute and State University

in partial fulfillment of the requirements for the degree of

Master of Science

in

Materials Engineering

APPROVED:

Dr. D.P.H. Hasselman, Chairman

Prof. H. R. Forkner

Dr. J. R. Thomas

September, 1987

Blacksburg, Virginia

**Thermal Conductivity/Diffusivity of SiC-Mullite and SiC-SiC Composites**

by

Laura M. Russell

Dr. D.P.H. Hasselman, Chairman

Materials Engineering

(ABSTRACT)

The purposes of this study were to determine as a function of temperature the thermal diffusivity and/or thermal conductivity of SiC-Mullite and SiC-SiC, and to explain the observed behavior in terms of changes in temperature, microstructure, composition, and/or orientation.

Materials used in the SiC-Mullite study consisted of single crystal SiC whiskers (prepared from rice hulls or by the vapor-liquid-solid process) dispersed within a polycrystalline mullite matrix. During measurement of thermal diffusivity, the samples were heated to 1500°C and cooled back to room temperature. No hysteresis occurred. However, both thermal diffusivity and conductivity exhibited maximum values at room temperatures, perpendicular to the hot pressing direction, at high volume percentages of SiC whiskers, and when VLS whiskers were employed.

The SiC-SiC samples consisted of a crossweave of polycrystalline SiC fibers that were coated with phenolic resin and surrounded by a chemically-vapor-deposited matrix of SiC. The two types of samples examined were prepared with different amounts of resin. The matrices of the high resin samples were found to be dominated by the presence of char. Samples were cycled to 1000, 1400, and

1800°C; hysteresis occurred on some of the cycles. Thermal diffusivity was highest parallel to one set of fibers.

These results allow the qualitative tailoring of the heat flow properties of these ceramic composites, for particular applications, and set forth limitations on the use of the SiC-SiC composites at high temperatures.

# Acknowledgements

I would like to thank my advisor for funding, and for provision of equipment. Thanks go to my committee members for their time and efforts at improving my thesis. Special thanks go to , , , and , for their moral support.

# Table of Contents

# List of Illustrations

# List of Tables

# Introduction

Recently, technical ceramics have begun to be used in a wide variety of applications. Their intrinsic properties of high hardness, strength, general stability with increasing temperature, resistance to chemical attack, and low densities make them attractive alternatives to some materials currently in use. The fracture toughness and thermal conductivity of ceramics are typically low. Low fracture toughness is a severe limitation in the use of ceramics as structural components. Fibers and whiskers have been added as reinforcing agents to the traditional monolithic ceramics in an effort to increase fracture toughness. The addition of such components is expected to affect the thermal conductivity.

The desired value of thermal conductivity for a material is low or high, depending on the particular application. Low values are desired when ceramics are used as thermal insulators, such as in furnace linings, adiabatic heat engines, or space shuttle tiles. High values are sought, for example, when ceramics are used as a circuit board material. With high values of thermal conductivity and elec-

trical resistivity, circuit boards inhibit the transport of electrons between electronic components while minimizing the overall temperatures. Notably, high thermal conductivity usually increases thermal stress resistance.

Exact prediction of thermal conductivity values for ceramics is very difficult. However, knowledge of the general principles involved allows the qualitative prediction of the effect of different factors on thermal conductivity. Thus ceramics materials can be tailored to fit a particular need.

## *General Principles of Heat Transfer*

Heat transfer through solids is governed by conduction, though radiation can contribute significantly at high temperatures. Thermal conduction involves the transfer of heat by phonons, and/or by electrons (1,2). All materials transfer heat by the movement of phonons, while only some materials allow the free movement of electrons. Typically, in ceramics the valence electrons are bonded tightly to the atoms, and thus thermal conductivity is dominated by phonon conduction.

K (thermal conductivity) is the coefficient between thermal flux and thermal gradient, as expressed by Fourier's Law:

$$Q = - KA(dT/dx) \qquad (1)$$

where Q is the amount of heat transferred per unit time through cross-sectional area A, and dT/dx is the thermal gradient (2).

Thermal diffusivity is related to thermal conductivity by:

$$K = \alpha \rho C_p \tag{2}$$

where $\alpha$ is the thermal diffusivity, $\rho$ is the density, and $C_p$ is the specific heat at constant pressure.

With increasing temperature, most materials expand and thus $\rho$ decreases. $C_p$ increases until at some high temperature specific to a material it levels off at a constant value. $C_p$ versus temperature curves are smooth unless phase changes, devolatization, or magnetic transitions occur in the material (3). In the temperature ranges of interest in this study (room temperature to 1800°C) both K and $\alpha$ are expected to decrease with temperature, as phonon interactions increase.

The thermal conductivity of a ceramic composite depends on the conductivity and spatial arrangement of its components. The addition of a second phase with thermal conductiviy different than the matrix can have a major effect on the effective thermal conductivity of the resulting composite (4). This effect was illustrated in a number of earlier studies (5-9) on whisker-reinforced glass, glass-ceramic and ceramic matricies. It was also found in the case of silicon carbide fiber-reinforced CVD-silicon carbide (6) that the thermal diffusivity was a function of thermal history due to the crystallization and change in chemical composition of the silicon carbide fibers at the higher temperatures. Furthermore, as indicated by the data for a uniaxially-carbon-fiber reinforced lithium-

alumina-silicate glass-ceramic (7), the thermal conductivity of brittle matrix composites also can be affected by the existence of a barrier to heat flow at the interface between the matrix and reinforcing fibers or whiskers. The effect of such an interfacial thermal barrier resistance on the effective thermal conductivity of composites was taken into account analytically (10), by extending the original theories of Raleigh (11) and Maxwell (12). It was also found (9) that composites with the same matrix but reinforced with different whiskers or fibers, can exhibit significant differences in their thermal conductivity and diffusivity. In turn, this provides an opportunity to tailor the heat conduction characteristics for candidate materials for a given application in a direction governed by design requirements.

The thermal conductivity of ceramics is measured by either transient or steady state methods (13). In steady-state methods, the distribution of temperature throughout the material is independent of time. Heat flow and temperature gradients are measured, and the thermal conductivity is calculated from equation (1).

In transient methods, the temperature distribution is a function of time. Temperature is varied suddenly or periodically at one part of the sample, and at a fixed distance away the change in temperature is measured. This process yields a value for the thermal diffusivity. Thermal conductivity may then be calculated from equation (2).

The purposes of this study are as follows:

1) To determine as a function of temperature the thermal diffusivity and/or conductivity of two sets of ceramic composites: SiC-Mullite and SiC-SiC.

2) To explain the observed behavior in terms of changes in temperature, microstructure, composition, and/or orientation.

# Equipment and Procedures

In this study, thermal diffusivity was measured using the transient laser-flash diffusivity method. This method was pioneered by Parker et al. (14). In this method, a small, thin disc-shaped sample is subjected to a laser pulse on one side. On the opposite side, the change in temperature with respect to time is monitored. The specimen thickness must be significantly less than the other dimensions to maintain one-dimensional heat flow. With the assumption of an instantaneous laser pulse, and uniform and one-dimensional heat flow, thermal diffusivity has been related to thickness of the sample (L), and the time it takes for the back face to achieve one half of its maximum temperature increase ($t_{1/2}$) by Parker et al. (14), as follows:

$$\alpha = .1388L^2/t_{1/2} \qquad (3)$$

The value of .1388 may be modified to account for indicated heat losses from the sample, according to Heckman (15). When $t_{1/2}$ is small, as with thin samples of high thermal diffusivity, a pulse duration effect must be considered (16).

The laser-flash diffusivity apparatus used in this study is illustrated in Figure 1. The Nd-glass laser generates a 800 microsecond pulse at a wavelength of 1.06 nm and variable energy per pulse of 30-55 J. In high temperature runs, the laser emits a pulse which is reflected off a mirror, through a quartz window, into a graphite resistance furnace, to impinge on one side of the sample. Inside the furnace an inert $N_2$ atmosphere is maintained. At temperatures $\leq$1000°C, a digital readout chromel-alumel thermocouple is used to measure ambient temperatures inside the furnace. At higher temperatures, an optical pyrometer is used.

On the bottom of the furnace, an optical detector is trained on radiation from the back of the sample, as viewed through a sapphire window. At temperatures from 300 to 700°C an InSb liquid nitrogen cooled infrared detector receives signals bounced off a gold surface mirror located below the furnace. At higher temperatures a Si-photodiode detector with a quartz lens is aimed directly at the specimen, through the sapphire window. The optical detector translates differences in temperature at the back face of the sample into voltage signals to a storage oscilloscope. For measurements at room temperature, the sample is mounted on the infrared detector, and receives direct unreflected emissions from the laser.

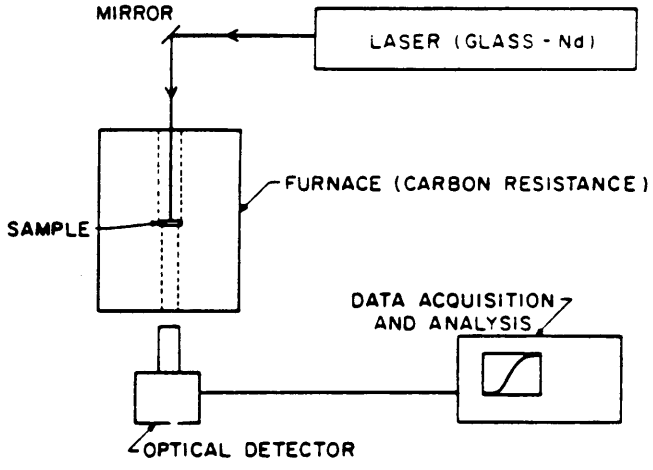


**Figure 1. Schematic of laser-flash diffusivity apparatus.**

A typical signal displayed on the oscilloscope is depicted in Figure 2. The baseline represents the equilibrium ambient temperature at the back face of the sample. The curve reflects the increase in temperature of the back face with time. The time it takes for the back face to achieve one half of its maximum temperature rise is read directly from the screen, and used to calcuate thermal diffusivity.

At each temperature, five measurements of $t_{1/2}$ were taken, to determine a mean value. Then heat-loss information was obtained, by measuring the maximum temperature increase and time, and the temperature increase at about ten times $t_{1/2}$. These values were then entered into a FORTRAN program run on an IBM/PC, along with sample thickness, ambient temperature, and the coefficient of thermal expansion. The program made finite pulse, heat-loss, and sample thickness corrections, then calculated the thermal diffusivity. In measurements at high temperatures, data were taken at 100°C intervals on heating, and 200°C intervals on cooling. Heatloss and thermal diffusivity values obtained as a function of temperature were used as input to a linear regression program, which fit a straight line through the heat-loss values, as a function of temperature, then adjusted the thermal diffusivity based on the new heat-loss values.

As part of the preparation for thermal diffusivity analysis, materials were cut into thin rectangular pieces with a slow speed circular diamond saw. After cutting, samples were thoroughly cleaned with acetone.

In some cases, density and heat capacity measurements were also obtained, to determine thermal conductivity. Density values were provided by the man-

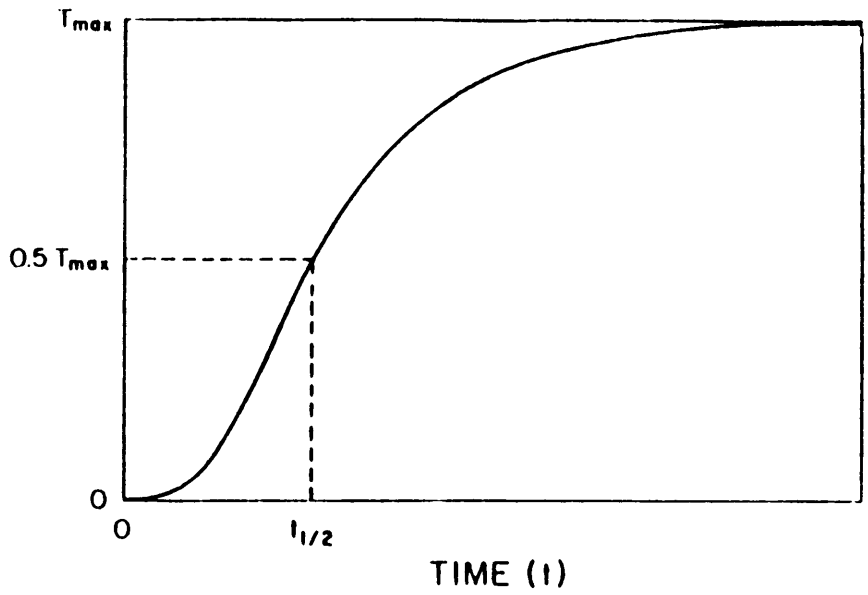


**Figure 2. Typical oscilloscope display:** transient temperature rise at the back face of a specimen which has been subjected to a heat pulse on its front surface.

ufacturer. Specific heat was measured on a differential scanning calorimeter (DSC). DSC measurements were made in nitrogen atmophere at constant atmospheric pressure. Thermal conductivity was then calculated from equation 2, with provision made for changes in density with temperature.

# Silicon Carbide Whisker Reinforced-Mullite Composites

## *Materials*

The SiC-Mullite composite samples were made by vacuum-hotpressing appropriate mixtures of alkoxide mullite (hydroxide suspensions of Al and Si) and silicon carbide whiskers at approximately 1700°C for 10 to 15 minutes in graphite dies at a pressure of about 35 MPa. The silicon carbide whiskers consisted of two types: 1) those made from rice-hulls (RH) [1] and 2) those made by the vapor-liquid-solid (VLS) process (17). In addition to the matrix phase without whiskers, the composite samples consisted of the matrix with 10, 20, and 30 w/o rice-hull whiskers and 30 w/o VLS-whiskers. Because the densities of silicon carbide and

[1] SC-9, ARCO Chemical Corp., Greer, S.C.

mullite are almost the same, weight and volume percent of the whiskers in these composites are almost the same. X-ray analysis showed that the composite samples contained a trace of alpha-alumina (18). It was found that the mullite in all hot-pressed samples exhibited a preferred orientation with the basal planes parallel to the hot-pressing direction. Due to the nature of material transport and flow during densification, the whiskers became preferentially oriented perpendicular to the hot-pressing direction. Table 1 lists the density, calculated percent of theoretical density as well as whisker type and content in the hot-pressed composites. Strength data for the composites with RH whiskers were presented elsewhere (19). Figure 3 shows a typical fractograph of a composite with 30% VLS SiC whiskers.

## *Results and Discussion*

The specimens consisted of ≅10 mm square platelets about 2 mm thick cut from the larger hot-pressed blocks. The specific heat to ≅600°C was measured by differential scanning calorimetry. The thermal conductivity, K, was then calculated from equation 2. Changes in specimen dimensions with temperature during the measurement of the thermal diffusivity due to thermal expansion and associated changes in density were taken into account using a value of $5 \times 10^{-6}$ $°C^{-1}$ for the coefficient of thermal expansion. For estimates of the thermal conductivity between 25 and 300°C, the corresponding values for the thermal

Table 1. Density, whisker type, and w/o SiC for SiC-Mullite samples.

| w/o SiC | Whisker Type | Density | % Theoretical |
|---|---|---|---|
| 0 | -- | 3.158 | 98.7 |
| 10 | SC-9 | 3.184 | 99.5 |
| 20 | SC-9 | 3.077 | 96.2 |
| 30 | SC-9 | 3.200 | 100.0 |
| 30 | VLS | 3.182 | 99.4 |

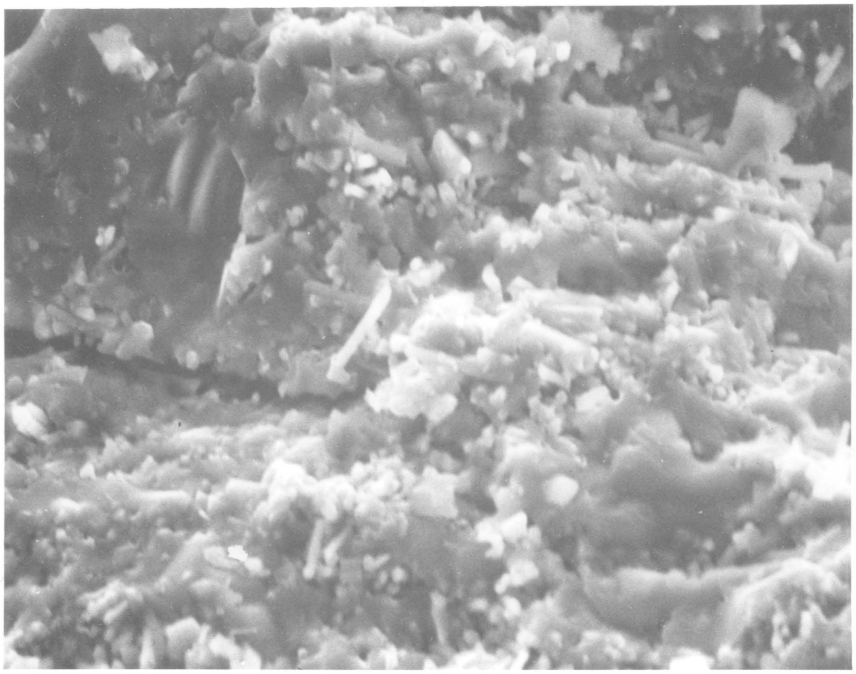

**Figure 3. SEM photograph of SiC-Mullite:** mullite matrix reinforced with 30 w/o silicon carbide VLS whiskers.

diffusivity were obtained by a fit of the experimental data assuming a 1/T dependence, where T is temperature in °K.

Figure 4 shows the experimental data for thermal diffusivity at room temperature as a function of whisker content. These data indicate that for both directions of heat flow the thermal diffusivity increases significantly with silicon carbide whisker content. This is to be expected because the thermal conductivity/diffusivity of dense silicon carbide (20-22) far exceeds the corresponding value for mullite (20,23,24). Also, the data show that the thermal diffusivity perpendicular to the hot-pressing direction significantly exceed the corresponding values parallel to the hot-pressing direction. The matrix shows isotropic behavior, so this effect most likely can be attributed to the preferred orientation of the whiskers within the composite samples. This conclusion agrees with theoretical expectations. Thus the effective thermal conductivity parallel to the plane or axis of preferred orientation of second-phase inclusions (in the form of platelets or cylinders) is expected to be higher than it is in the transverse direction (4).

Most interesting is the observation that the composite with 30 w/o VLS whiskers exhibits a value for thermal diffusivity considerably higher than the value for the composite with 30 w/o rice-hull whiskers. Such differences can be attributed only to differences in the thermal conductivity/diffusivity of the whiskers, as for all composite samples the matrix phase and processing conditions were identical. Such differences in the heat conduction behavior of the whiskers

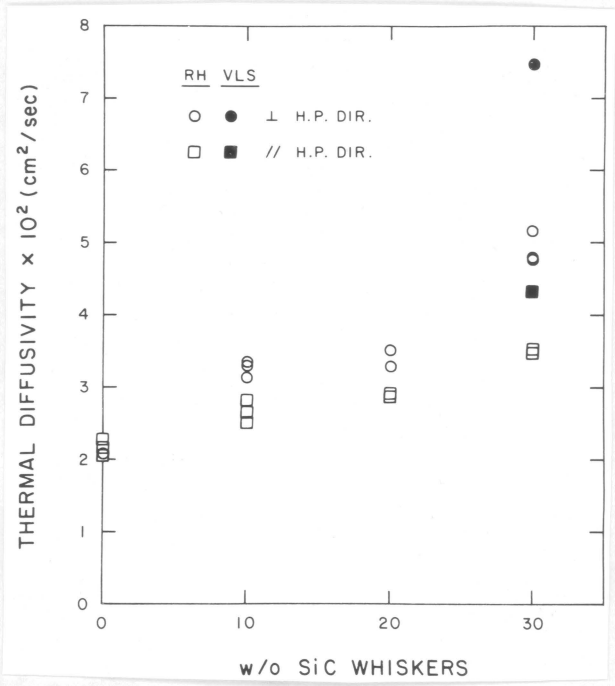


**Figure 4. Room temperature thermal diffusivity of SiC-Mullite:** mullite matrix reinforced with rice-hull (RH) and vapor-liquid-solid (VLS) silicon carbide whiskers perpendicular and parallel to the hot-pressing direction as a function of whisker content.

most likely can be attributed to the presence of voids and much higher densities of crystalline defects in the rice-hull whiskers than in the VLS whiskers (25,26).

Using composite theory, an estimate can be made of the thermal conductivity of the whiskers from the corresponding values for the matrix, with or without whiskers. For this purpose the data for thermal conductivity for the matrix and composite samples were calculated from the mean values of the thermal diffusivity shown in Figure 2, the data for the density given in Table 1 and the data for the specific heat listed in Table 2. These data show that the specific heat does not depend strongly on whisker content or type, as expected, because the values for specific heat for mullite and silicon carbide are comparable (27).

The resulting values of thermal conductivity are shown in Figure 5, together with curves for the effective thermal conductivity of composites as a funtion of volume fraction of dispersions consisting of noninteracting circular cylinders oriented perpendicularly to the heat flow for a range of values of the ratio $\frac{K_d}{K_m}$. $K_d$ and $K_m$ are the values of the thermal conductivity of the dispersions and matrix, respectively. For the composite samples with the rice-hull whiskers a good match between the theoretical and experimental data is obtained at a value of $\frac{K_d}{K_m} \cong 5$. This implies that with $K_m \cong 5.2$ W/m °K, the value of the thermal conductivity of the silicon carbide whiskers is about 26 W/m °K with a corresponding value of the thermal diffusivity of $\cong 0.1$ cm$^2$/sec. This value is much lower than the values for the thermal diffusivity ranging from $\cong 0.25$ to $\cong 1.0$ cm$^2$/sec obtained (personal communication, 1987, D.P.H. Hasselman) over the last few years for a variety of dense structural silicon carbides, impure and high-

Table 2. Specific heat (J/g °C) of SiC-Mullite.

| Temperature °C | % Rice Hull Whiskers | | | | VLS Whiskers |
|---|---|---|---|---|---|
| | 0 | 10 | 20 | 30 | 30 |
| 25 | 0.767 | 0.753 | 0.746 | 0.735 | 0.746 |
| 100 | 0.894 | 0.880 | 0.878 | 0.866 | 0.878 |
| 200 | 1.002 | 0.990 | 0.991 | 0.980 | 0.988 |
| 300 | 1.073 | 1.063 | 1.061 | 1.052 | 1.063 |
| 400 | 1.095 | 1.116 | 1.111 | 1.106 | 1.108 |
| 500 | 1.139 | 1.153 | 1.149 | 1.139 | 1.142 |
| 595 | 1.185 | 1.176 | 1.187 | 1.165 | 1.174 |

purity crystalline silicon carbides. The low value for the thermal diffusivity of the rice-hull whiskers is indicative of the effectiveness of the pores and stacking faults in lowering the thermal conductivity of the rice-hull whiskers from a value expected for pure crystalline silicon carbide. It is of interest to note that the value of thermal diffusivity ($\cong 0.1$ cm$^2$/sec for the rice-hull whiskers as inferred from the experimental data) is in excellent agreement with the same value inferred from data for rice-hull silicon carbide whisker reinforced polycrystalline aluminum oxide (of $\cong 0.1$ cm$^2$/sec). This shows that the thermal diffusivity was not affected by the whiskers (28). This in turn suggests that the thermal diffusivity of the whiskers is comparable to that of the alumina matrix.

In Figure 5, the data point for the thermal conductivity of the composite sample of mullite reinforced with 30 w/o VLS silicon carbide whiskers lies slightly above the curve for $\frac{K_d}{K_m} = \infty$. This implies that the thermal conductivity of the VLS whiskers is very high compared to the mullite matrix. The theoretical curves in Figure 5 were based on the assumption that the whiskers were oriented exactly perpendicularly to the hot-pressing direction. However, a fraction of whiskers are oriented in the hp-direction, which would tend to increase the corresponding thermal conductivity and diffusivity. For this reason, the theoretical curves in figure 5 tend to be underestimates. For the same reason the values for the thermal conductivity of the whiskers inferred from these curves tend to be overestimates. Because the curves for $10 < \frac{K_d}{K_m} < \infty$ are very closely spaced, an estimate for the thermal conductivity of the VLS whiskers much higher than for

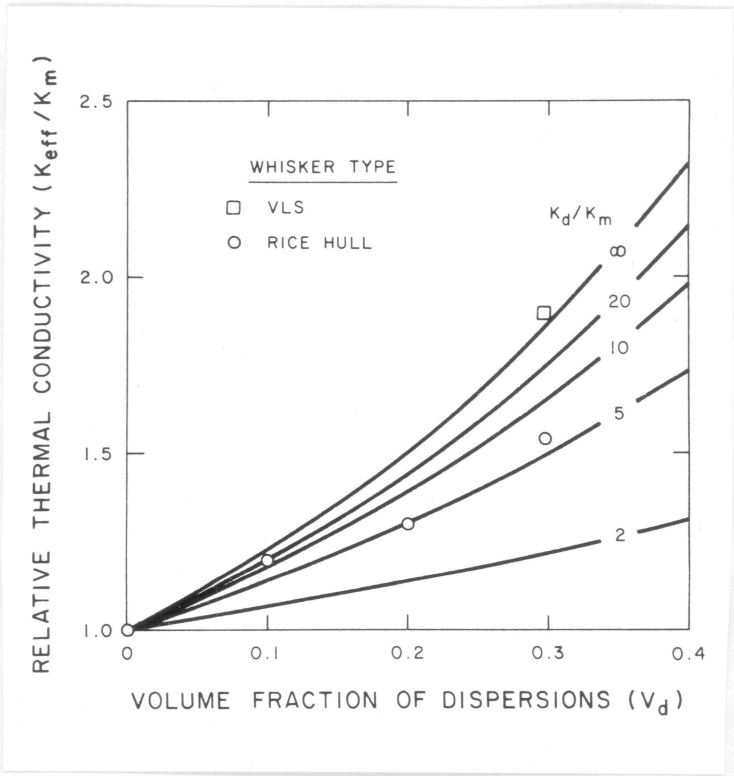


**Figure 5. Theoretical and experimental variation in thermal conductivity:** comparison of relative changes in thermal conductivity at room temperature of silicon carbide whisker-reinforced mullite with those predicted by composite theory.

the matrix cannot be considered very precise. For this a matrix with thermal conductivity comparable to the VLS whiskers is required.

Figures 6 and 7 show temperature vs. thermal diffusivity for the mullite matrix and the composite samples with rice-hull and VLS whiskers for both directions of heat flow relative to the hot-pressing directions. Similarly, Figures 6a and 6b show the corresponding data for the thermal conductivity. Figures 6 through 8 indicate that the increase in thermal diffusivity and conductivity with increasing whisker content is maintained to the highest value of the temperature at which the measurements were made. Qualitatively the thermal diffusivity and conductivity exhibit a negative temperature dependence. Quantitatively the thermal conductivity shows a smaller negative temperature dependence, because it reflects both the negative temperature dependence of the thermal diffusivity and the positive temperature dependence of specific heat.

In summary, in this study it was seen that both thermal diffusivity and conductivity were maximized: at low temperatures, perpendicular to hot pressing, at high volume percentages of SiC whiskers, and when VLS whiskers were employed. From the perspective of materials development and selection, with these results the heat conduction behavior of whisker-reinforced composites can be tailored in a direction to optimize design requirements.

a.

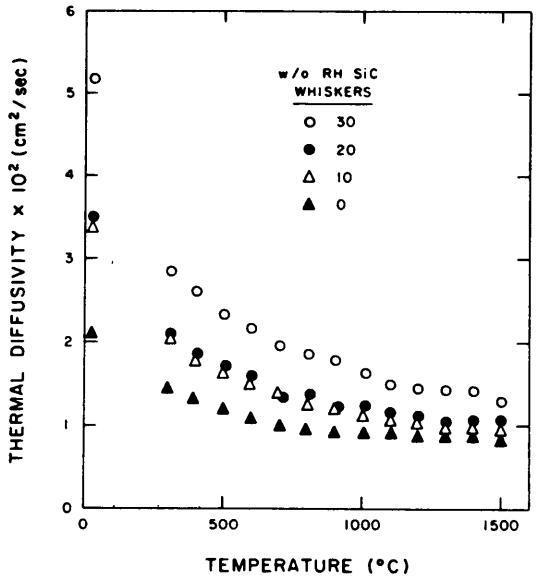


b.

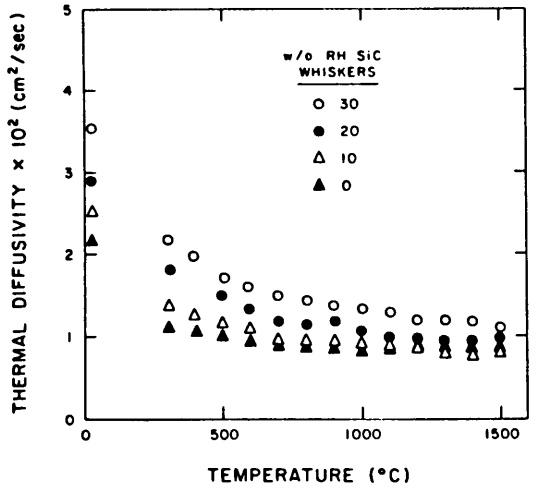


**Figure 6. Changes in thermal diffusivity with temperature, RH SiC-Mullite:** temperature dependence of the thermal diffusivity of rice-hull silicon carbide whisker reinforced mullite for a range of values of whisker content, a: perpendicular and b: parallel to hot-pressing direction.

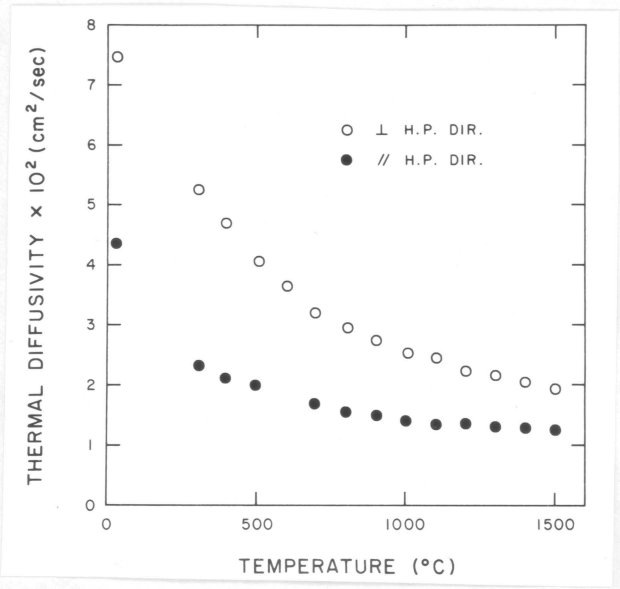


**Figure 7. Changes in thermal diffusivity with temperature, VLS SiC-Mullite:** temperature dependence of the thermal diffusivity of a mullite matrix reinforced with 30 w/o VLS silicon carbide whiskers.

a.

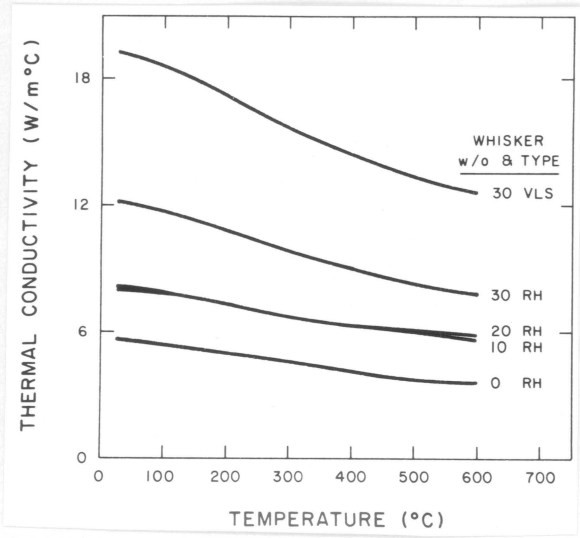


b.

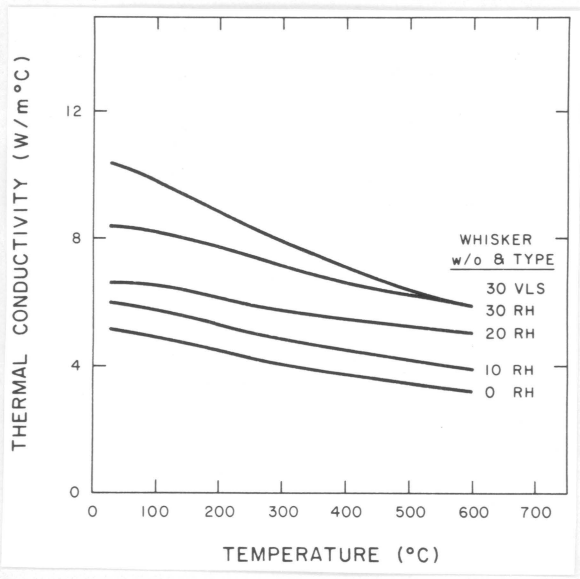


**Figure 8. Changes in thermal conductivity with temperature:** temperature dependence of the thermal conductivity of mullite reinforced with rice-hull (RH) or vapor-liquid-solid (VLS) for range of whisker content, a: perpendicular and b: parallel to hot-pressing direction.

# Silicon Carbide-Silicon Carbide

## *Materials*

Two sets of SiC-SiC ceramic composite samples were examined in this study. Each consisted of a bidirectional weave of SiC fibers surrounded by a SiC matrix. During processing, the SiC fibers were coated with a phenolic resin, then inserted as a preform into a chemical vapor deposition (CVD) chamber. There an organic carrier gas was passed over the substrate, and a matrix of crystalline SiC was deposited on and around the crossweave. This occurred at $\cong 1000°C$; at these high temperatures, the phenolic resin reacts to form a carbon-rich residue, known as char. These samples were manufactured by the Refractory Composites Institute (RCI).

The two sets of samples differ in the amount of phenolic resin that was used to coat the fibers, and in the resultant amount of char that was present in the

composite. One set of samples contained about 2 volume percent char, while the other contained about 15 volume percent (personal communication, 1987, Jim Warren, RCI). Hereafter these samples will be referred to as low and high char samples, respectively. Fibers are coated to weaken bonding between the fiber and the SiC matrix, and thereby promote fiber pull-out upon fracture. This tends to increase the fracture toughness of the samples.

Distinct differences were found between the two types of samples, after examination with a scanning electron microscope. Figures 9 and 10 display fracture surfaces of high and low char samples, respectively. On fracture in the high char samples, the fibers tended to separate from the matrix. In contrast, the low char samples (with better bonding between fibers and matrix) tended to experience planar fracture. Another difference involved the appearance of the matrix immediately surrounding some of the fibers. In low char samples, fibers were typically rimmed by concentric rings, as seen in Figure 10. This is a typical structure for CVD samples, and represents successive depositional layers around the fibers. These rings were not detected in the high char samples.

Figure 11 displays spherical particles found in the low and high char samples. The coarser particles seen in the high char sample are believed to be particles of char. The finer particles found in the low char sample are believed to be CVD SiC matrix particles.

These samples were examined further, in particular to distinguish between the low and high char samples, as they were received from the manufacturer. With reflected light microscopy (Figure 12) it was seen that the low char sample

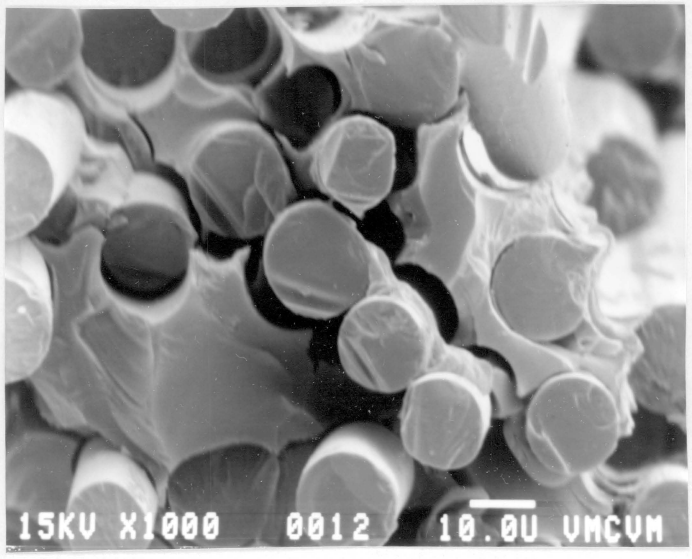


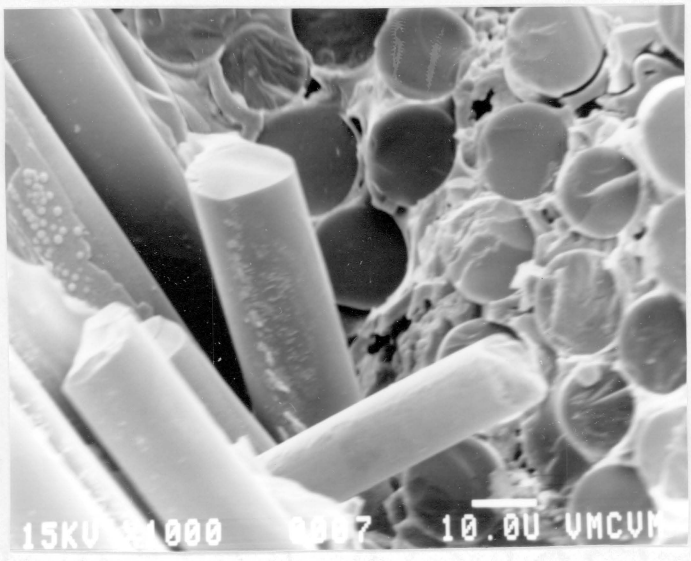


**Figure 9. Fracture surfaces of high char samples:** shows typical behavior of separation of fibers from matrix on fracture.

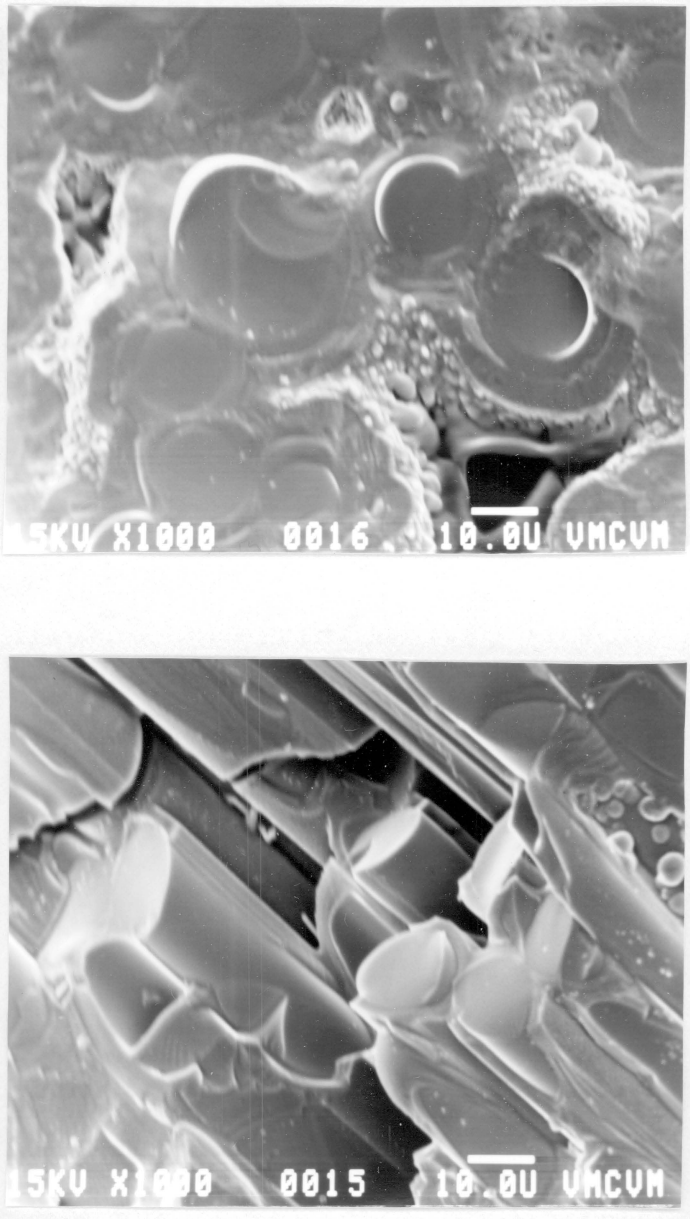


**Figure 10. Fracture surfaces of low char samples:** good bonding between fibers and matrix has resulted in planar fracture.

a.

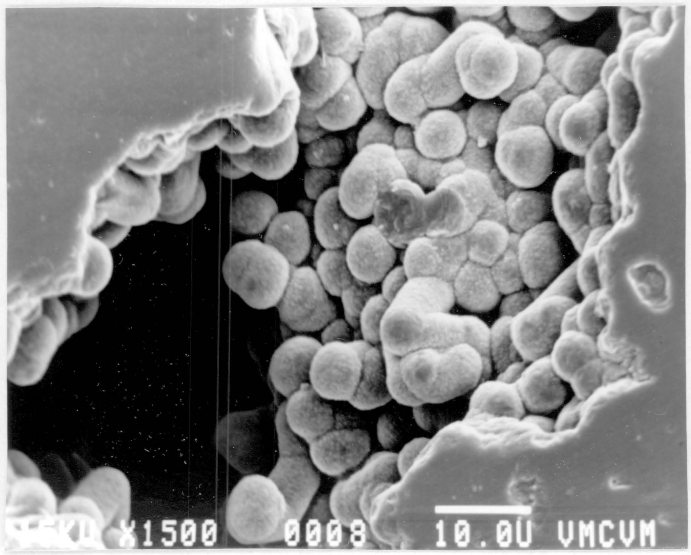


b.

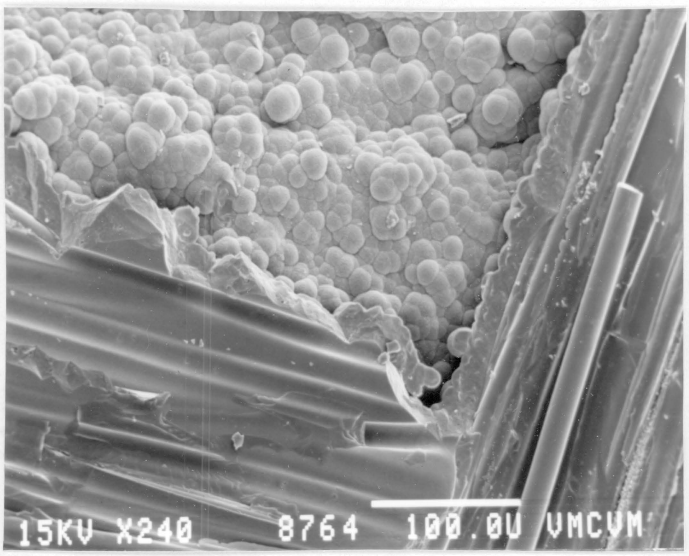


**Figure 11. Spherical particles in low and high char samples:** in a: the low char sample, they are believed to be matrix particles, while in b: the high char sample, they are thought to be char.

consisted of three distinct components: pores, fibers, and matrix. The light-colored matrix phase apparently deposited itself evenly in rings around the fibers. The high char samples (Figures 13 and 14) were found to contain all of the above, plus one other distinct component: the char. The char occupies a significant volume of the material, and is found clustered around the fibers. Deposition of the matrix apparently took place primarily in pores (Figure 13) and on the outer edges of the sample (Figure 14).

Further elucidation occurred with back scattered electron (BSE) imagery and with elemental mapping (Figures 15-17). The BSE image of the low char sample shows three distinct components: pores, the fibers, and the matrix. In BSE imagery, compounds with higher average atomic weights show up as lighter shades on the photograph. So the matrix in the low char sample has a higher average atomic weight than the fibers. The matrix is found as concentric rings around the fiber and thickly on the edge of the sample. In the BSE image of the high char sample, pores, fibers, SiC matrix, and the char are all seen. The pores are difficult to distinguish from the char, as both are quite dark. The char is the predominant matrix material in this composite. Neglecting the pores, it is the darkest component and therefore has the lowest average atomic weight. The SiC matrix is seen as a heavy concentration on the edge of the high char samples and as convoluted strands throughout the material. As in the low char sample, the matrix is a lighter shade than the fibers.

Normally, in elemental mapping, when the element to be analyzed is present it shows up as light dots on the photo. This occurs unless the wavelength of the

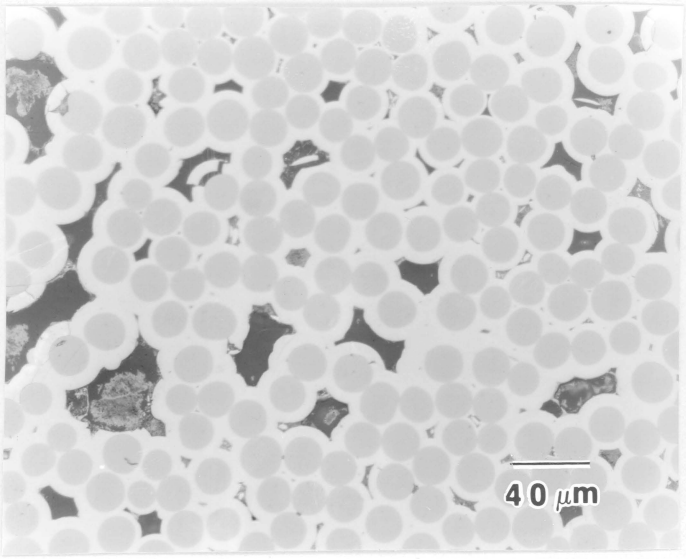


**Figure 12. Reflected light photo of low char SiC-SiC composite:** fibers are rimmed by lighter colored matrix, and dark colored pores are scattered throughout the sample.

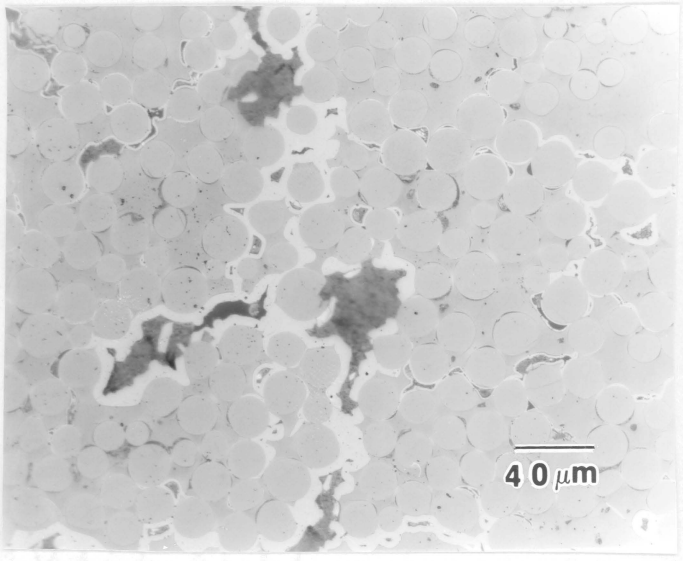


**Figure 13. Reflected light photo of high char SiC-SiC composite:** light colored matrix is concentrated in pores, and fibers are mostly surrounded by darker colored char.

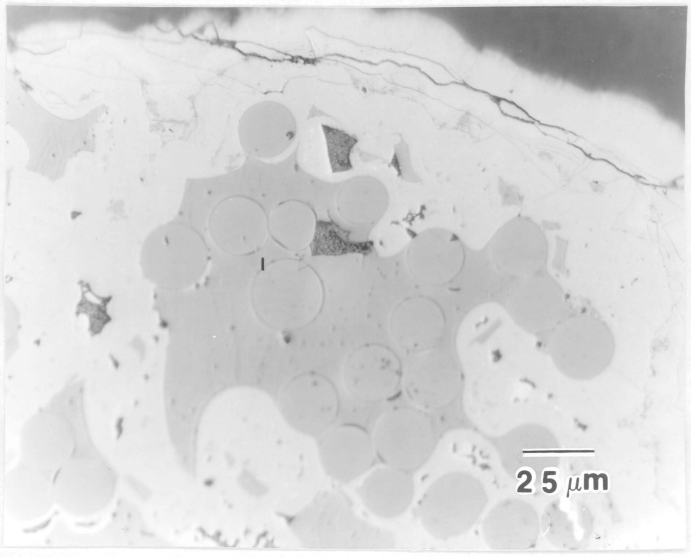


**Figure 14. Reflected light photo of high char SiC-SiC composite:** shows high concentration of light colored matrix on edge of sample.

a.

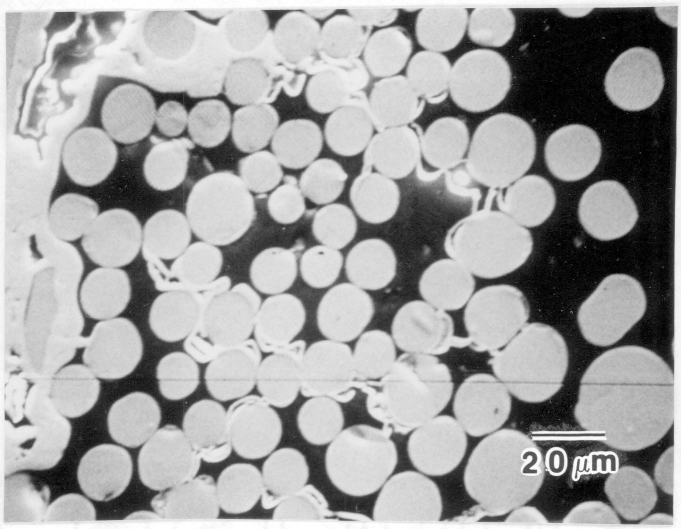


b.

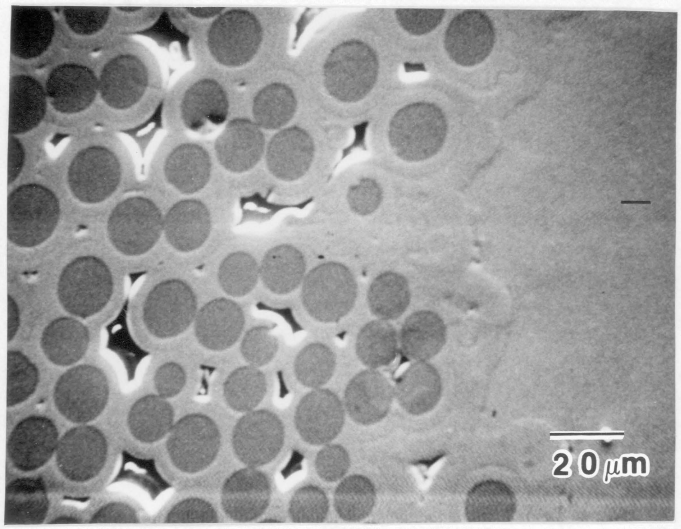


**Figure 15. BSE images of high and low char samples:** in a: the high char sample, fibers are surrounded by dark colored char, and light colored CVD SiC is seen on edge of sample; in b: the low char sample, light colored CVD SiC is seen rimming fibers and on edge of sample.

a.

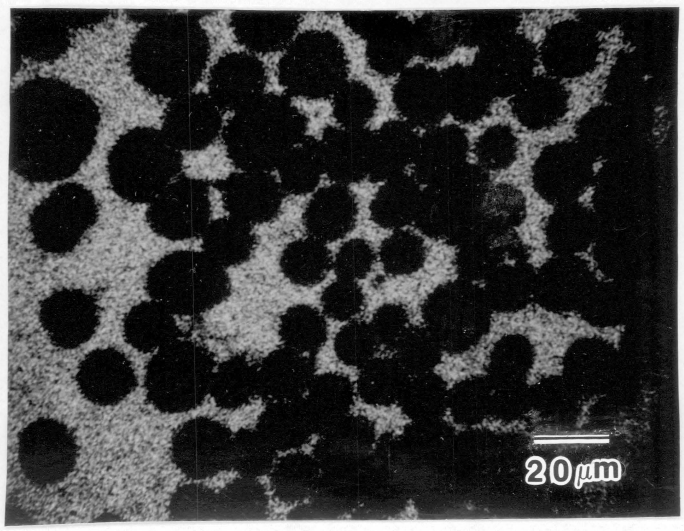


b.

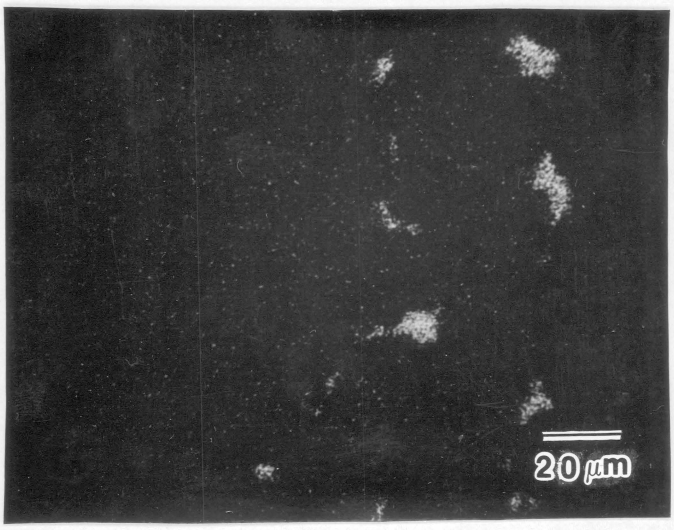


**Figure 16. Carbon maps of high and low char samples:** in a: the high char sample, fibers are surrounded by carbon-rich matrix; in b: the low char sample, little carbon is detected.

a.

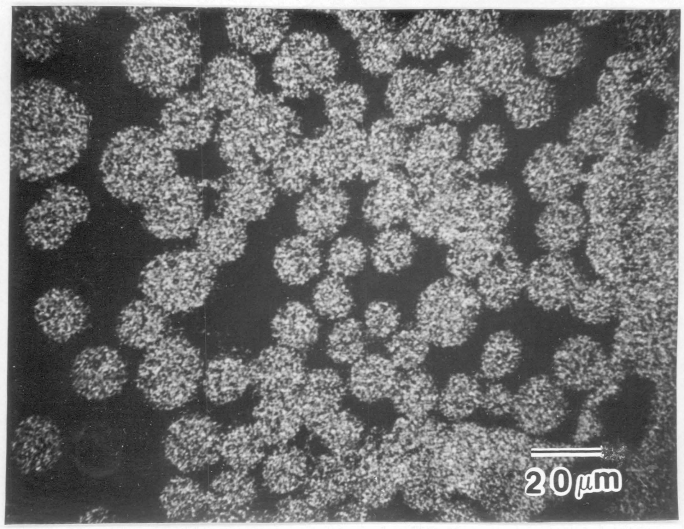


b.

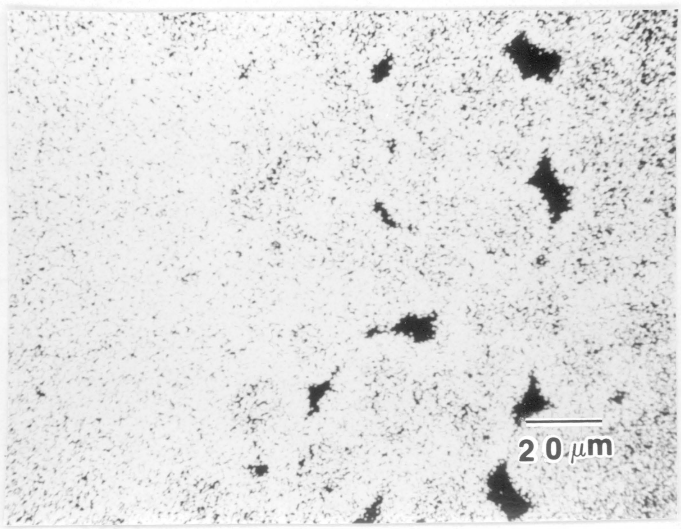


**Figure 17. Silicon maps of high and low char samples:** in a: the high char sample, Si-rich fibers are surrounded by Si-poor matrix; in b: the low char sample, Si is distributed evenly throughout the sample, except in pores.

x-rays generated from the element of interest matches the absorption edge of a neighboring element. Carbon x-rays are absorbed by silicon. So on a carbon map of the materials in this study, carbon found in char-rich areas should show up as light dots, while carbon present in a SiC compound will not.

There is a dramatic difference in the elemental images of the low and high char samples (Figures 16 and 17). The carbon image of the high char sample shows dark fibers surrounded by a carbon-rich matrix, while the carbon map of the low char sample is almost completely and uniformly dark. The silicon maps show a low char sample rich in silica, and a high char sample with silicon-rich fibers surrounded by a Si-poor matrix.

The reflected light, BSE, and elemental mapping analyses suggest that the high char samples are primarily a SiC fiber-char matrix composite.

## *Results and Discussion*

Half of the samples were cut so that the incident laser flash would be perpendicular to the fibers, while half were cut so that heat would flow parallel to one set of the fibers. Changes in specimen thickness with temperature during the measurement of the thermal diffusivty due to thermal expansion were taken into account using a value of $4 \times 10^{-6}$ °$C^{-1}$ for the coefficient of thermal expansion.

Room temperature thermal diffusivity values for both high and low char samples, perpendicular and parallel to the fibers, are shown in Figure 18. In both

types of samples, thermal diffusivity was lower perpendicular to the fibers than it was parallel. This is in accordance with general composite theory (4), which predicts that, no matter what the relative thermal conductivities of two different structural components, parallel to an aligned set of fibers the thermal conductivity will be higher than in any other orientation.

It is also seen in Figure 18 that thermal diffusivity perpendicular to the fiber plane for both types of samples is approximately the same. However, parallel to the fibers the thermal diffusivity for the low char samples is consistently higher than for the high char samples. This is unexpected, since heat flow parallel to one set of the fibers is being carried by the fibers, and the same type of fiber was used in each type of composite. It is possible that the batch of fibers used in the manufacture of the low char samples was simply of higher quality than the batch used to make the high char samples. Scatter among samples of the same type and orientation is understandable and expected, as samples came from different areas in the CVD block, and these composites typically vary with location in the block (6).

Figures 19 and 20 display thermal diffusivity as a function of temperature, as the samples were heated to 1000°C and cooled back to room temperature. Both sets of samples show similar results. Thermal diffusivity perpendicular to the fiber plane remained consistently lower than thermal diffusivity parallel to the fiber plane. In addition, heating of the samples produced no permanent changes in thermal diffusivity on cooling. In the low char samples, thermal diffusivity decreased slightly with temperature. Parallel to the fiber plane the rate of de-

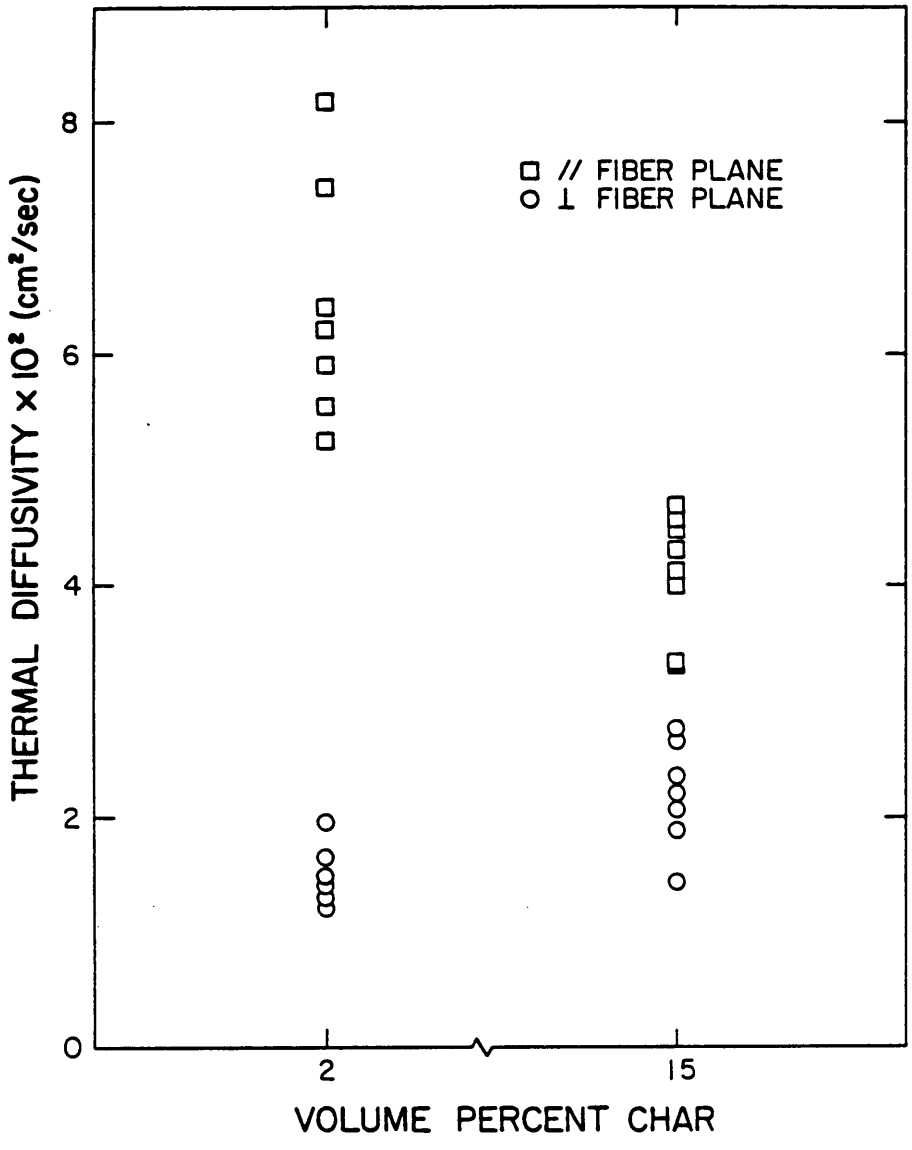


**Figure 18. Room temperature thermal diffusivity of SiC-SiC composites:** in samples with low and high char contents, parallel and perpendicular to the fiber plane.

crease was maintained though lessened up to 1000°C, while perpendicular to the fiber plane the slope levelled off quickly above 300°C then became slightly positive. In the high char samples, thermal diffusivity decreased with temperature until about 600°C, when it began to increase slightly. Normally, in this temperature range phonon conduction is inversely proportional to temperature. However, photon conduction is directly proportional to the third power of temperature. At the higher temperatures radiation across large pores may be causing the increase in thermal diffusivity.

Somewhat similar results were attained on heating and testing of the samples to 1400°C, as seen in Figures 21 and 22. Again, in both sets of samples thermal diffusivity perpendicular to the fiber plane remained lower than in the parallel direction. In both orientations of the low char samples, thermal diffusivity decreased with increasing temperature, then tended to level off. However in both of the high char samples, above about 600°C, thermal diffusivity increased with temperature. This increase was retained on cooling in the parallel high char sample; the room temperature thermal diffusivity was 21% higher than the initial room temperature value. This suggests some annealing effects in the sample, and may be attributed to some change in the fibers themselves, as no annealing effects were seen perpendicular to the fibers.

Figures 23 and 24 show thermal diffusivity values on heating to 1800°C and cooling back to room temperatures. Again, as expected, thermal diffusivity in the low char samples parallel to the fibers is higher than it is perpendicular to the fiber plane. However, the perpendicular high char sample, after heating to

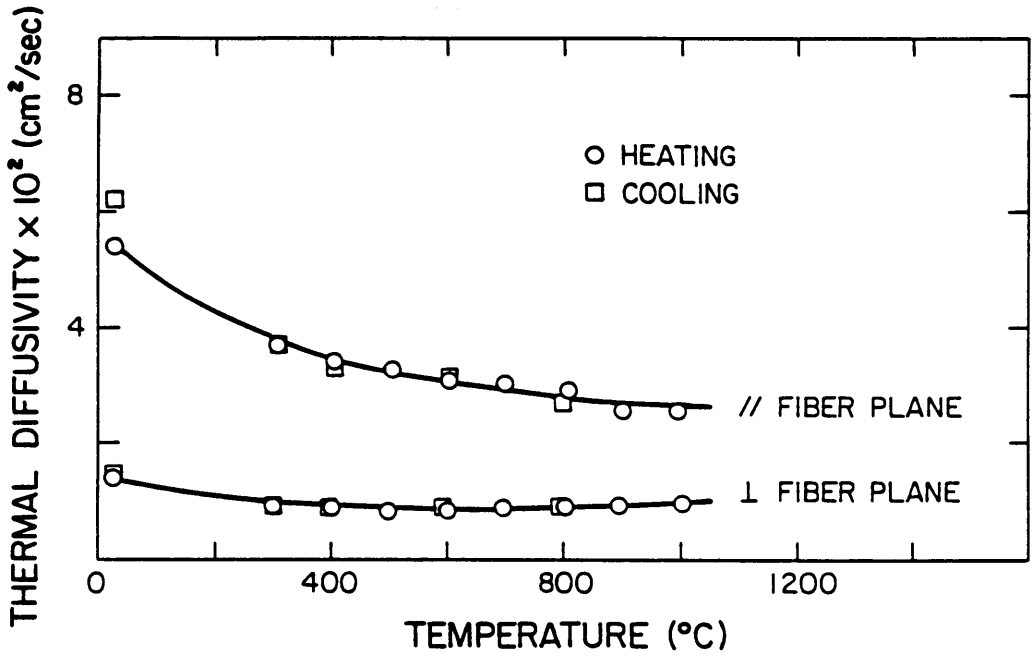


**Figure 19. Changes in thermal diffusivity to 1000°C, low char samples:** shows effect of thermal cycling to 1000°C, parallel and perpendicular to the fiber plane.

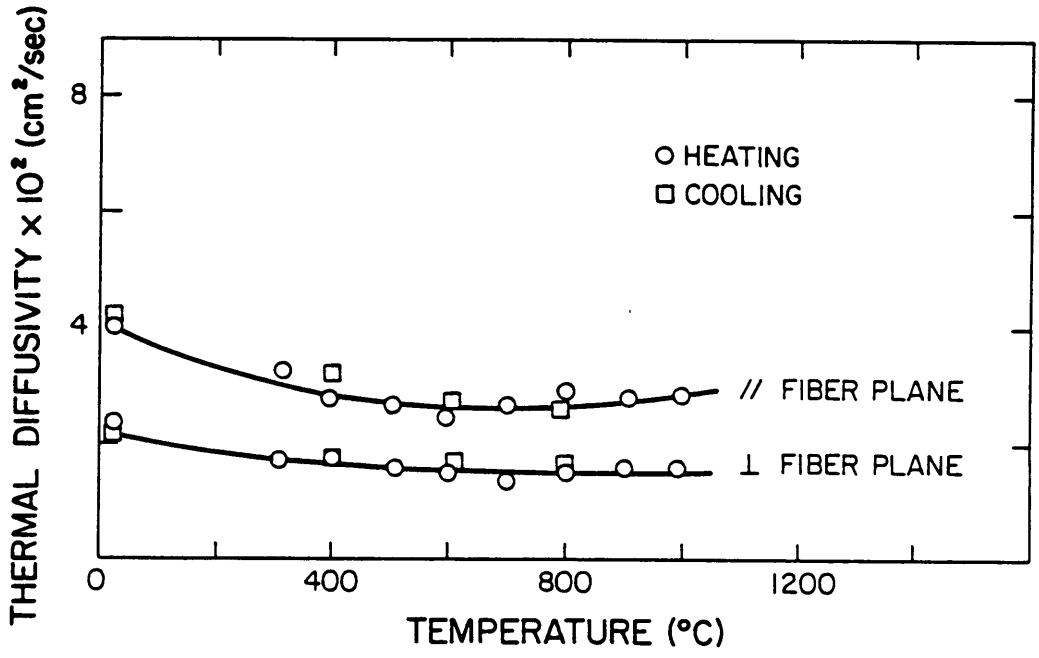


**Figure 20. Changes in thermal diffusivity to 1000°C, high char samples:** shows effect of thermal cycling to 1000°C, parallel and perpendicular to the fiber plane.

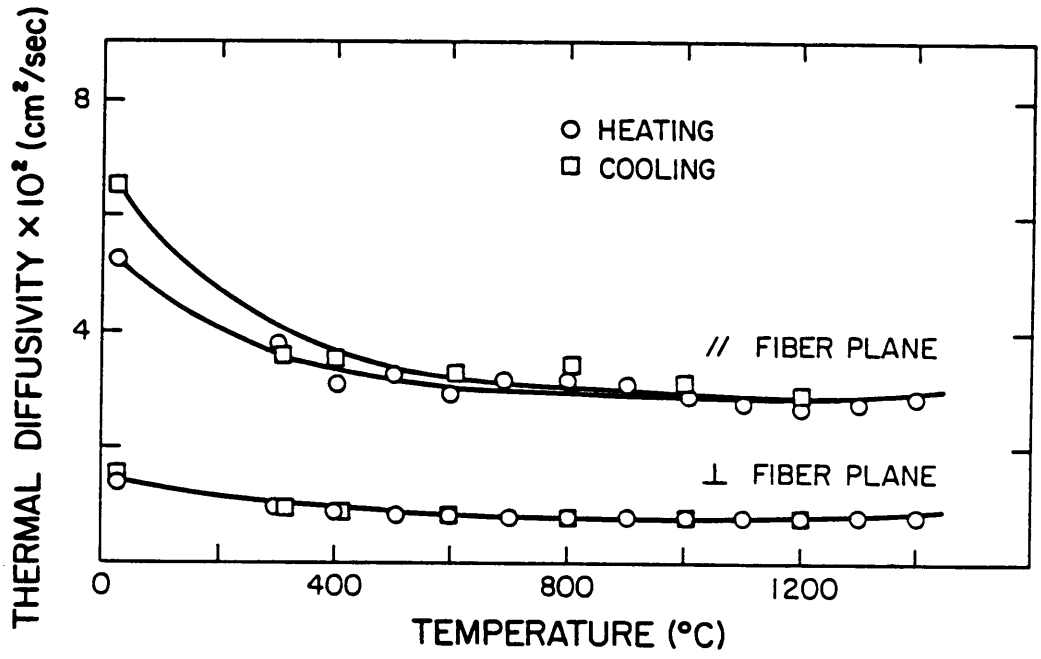


**Figure 21. Changes in thermal diffusivity to 1400°C, low char samples.:** shows effect of thermal cycling to 1400°C, parallel and perpendicular to the fiber plane.

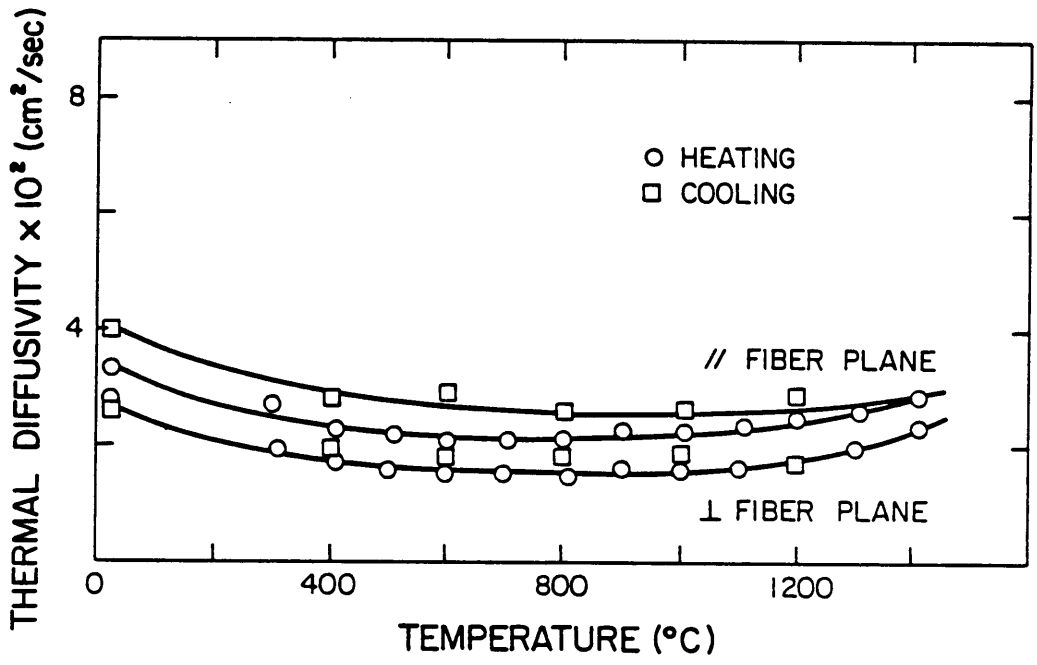


**Figure 22. Changes in thermal diffusivity to 1400°C, high char samples:** shows effect of thermal cycling to 1400°C, parallel and perpendicular to the fiber plane.

1800°C, and cooling to below 1200°C , exhibited a higher thermal diffusivity than the original parallel high char sample. All samples, on experiencing this heat treatment, showed significant increases in thermal diffusivity. In the high char samples, the room temperature thermal diffusivity increased by 257% and 347% for the perpendicular and parallel orientations, respectively. In the low char samples, room temperature thermal diffusivity increased by 178% and 222% for the perpendicular and parallel orientations, respectively. Thus annealing effects were more pronounced parallel to the fibers, and in the high char samples. In the high char samples, thermal diffusivity began to increase above about 700°C perpendicular to the fiber plane, and above 900°C parallel to the fibers. In the low char samples, increases were seen above about 700°C perpendicular to the fiber plane, but not until above 1400°C parallel to the fibers. It is possible that increases in thermal diffusivity perpendicular to the fiber plane arise from crystallization of the char. Differences in annealing effects between the low and high char samples may possibly be due to differences in time spent at temperature during the analysis of those samples. Unfortunately, no records of this were kept.

Figure 25 shows SEM photos of the polished surfaces of a high and a low char sample after heating to 1800°C. The altered appearance of these fibers, as compared with the unheated fibers seen in Figures 9 and 10, is evidence of degradation at high temperatures.

X-ray diffraction (XRD) patterns were recorded for four of the samples, from 2θ angles of 20 to 90°. During analysis K-β peaks were filtered out, so only the K-α peaks were recorded. Each recording represented a direct comparison

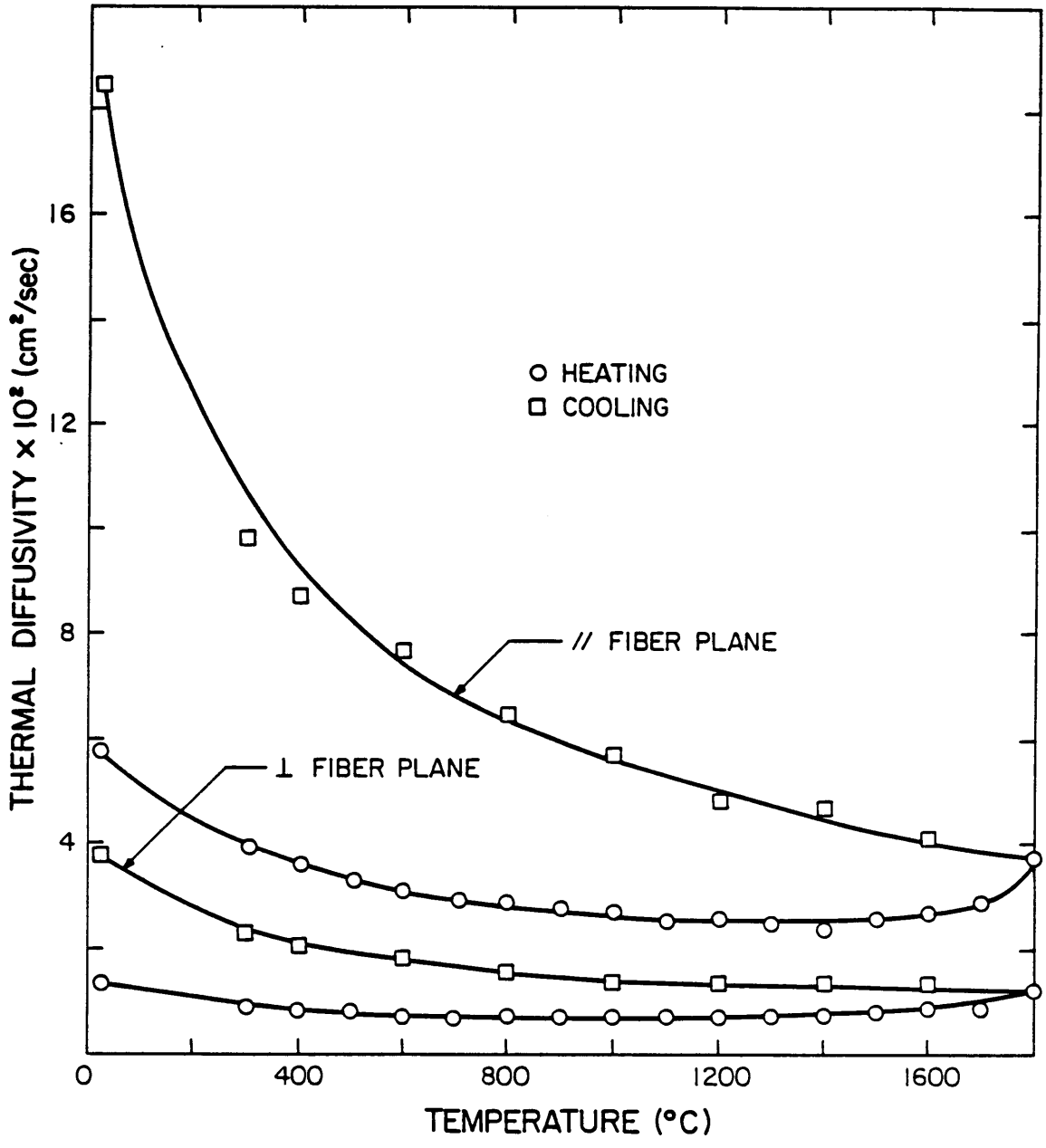


**Figure 23. Changes in thermal diffusivity to 1800°C, low char samples:** shows changes in thermal diffusivity on thermal cycling to 1800°C, both parallel and perpendicular to the fiber plane.

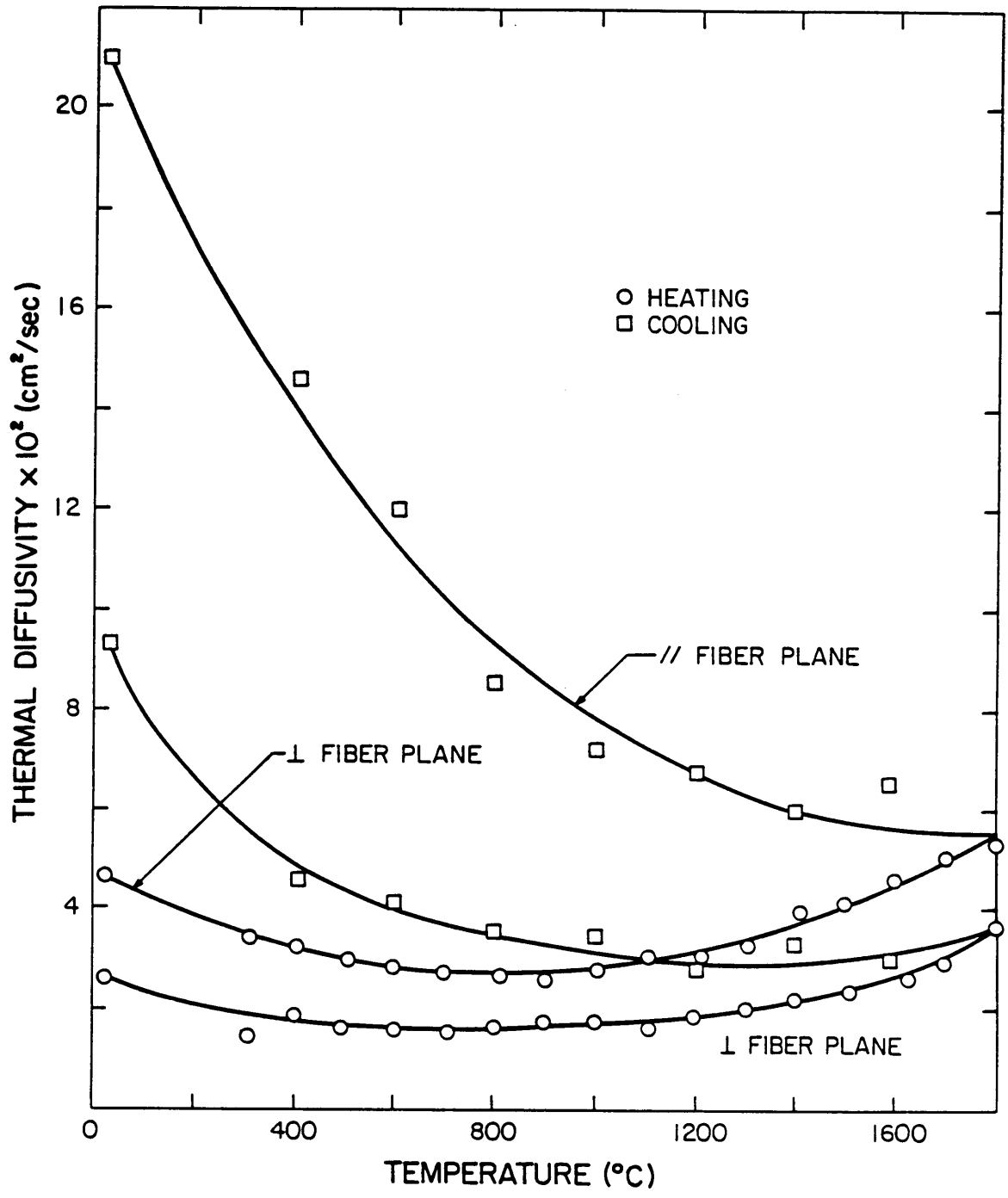


**Figure 24. Changes in thermal diffusivity to 1800°C, high char samples:** shows changes in thermal diffusivity on thermal cycling to 1800°C, both parallel and perpendicular to the fiber plane.

a.

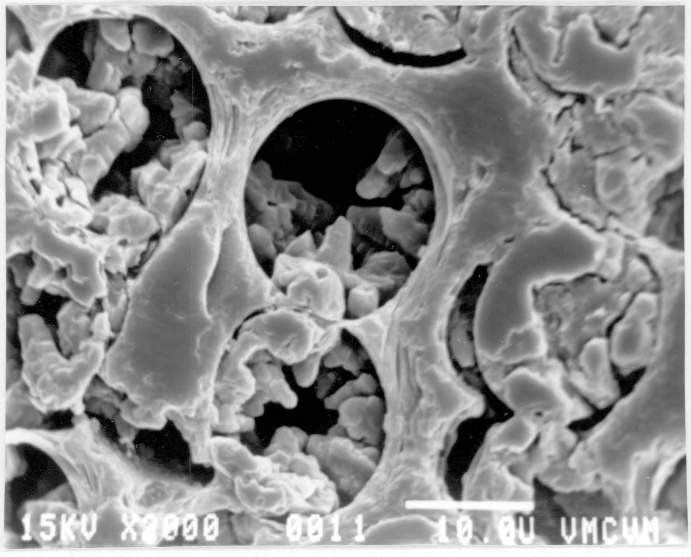


b.

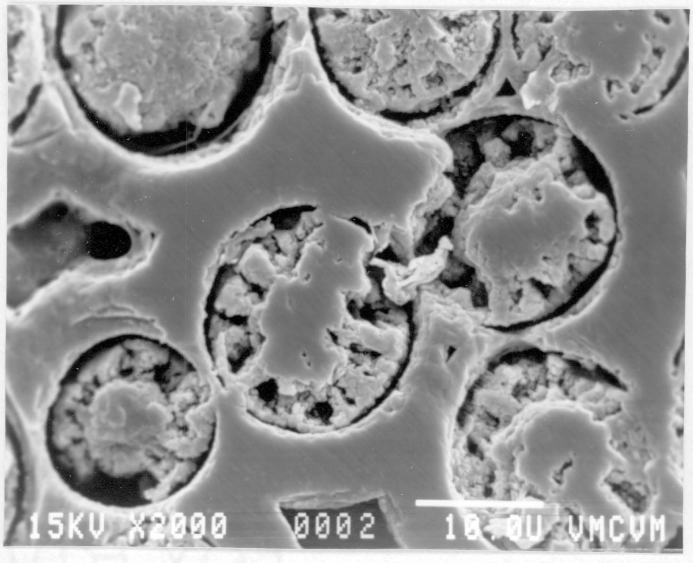


**Figure 25. SEM photos of polished surfaces of annealed samples:** shows effect on fibers after thermal cycling to 1800°C, in a: high char sample, and b: low char sample.

between a high or low char sample as received and the same type of sample after heating to 1800°C. Analyses of the peaks that were obtained for these samples are displayed in Tables 3 and 4.

The diffraction patterns obtained for the as-received low and high char samples are quite similiar. In both cases only two peaks of relatively low intensity were obtained. However, it is clear that these are SiC peaks. In the annealed samples, these two peaks are also found, but they are sharper and more intense. The additional peaks that appear in the diffraction patterns of the heated samples are SiC peaks, plus two unknown peaks in the high char sample. The patterns obtained for the heated samples most closely resemble those found for the β cubic polymorph of SiC. The two unknown peaks found in the heated high char sample may represent some crystalline compound associated with high temperature reactions in the char phase.

As discussed by Cullity (29), XRD peaks generally become sharper and more intense due to: 1. removal of nonuniform strains 2. amorphous to crystalline transformations and/or 3. increases in grain size. Point one is considered unlikely, since ceramics do not generally accommodate strains and these composites were formed at room pressure and low stresses. In regard to point 2, since SiC peaks were obtained for the as-received samples in this study, at least some of the SiC in those samples is crystalline. Other workers have found that both SiC formed during chemical vapor deposition, and SiC in fibers is crystalline (30-34). Mah et al. (30) did a comprehensive study on the effects of heat treatment on SiC fibers, and found that at temperatures > 1200°C SiC fibers tended

Table 3. Analysis of XRD peaks for the low char samples

| Sample | 2θ | d(Å) | Intensity | Identification |
|---|---|---|---|---|
| As-received | 35.65 | 2.51 | 73 | SiC |
| | 60.10 | 1.54 | 47 | SiC |
| After Heating | 35.65 | 2.51 | 319 | SiC |
| | 60.05 | 1.54 | 75 | SiC |
| | 72.85 | 1.30 | 37 | SiC |

Table 4. Analysis of XRD peaks for the high char samples

| Sample | 2θ | d(Å) | Intensity | Identification |
|---|---|---|---|---|
| As-received | 35.70 | 2.51 | 30 | SiC |
| | 60.15 | 1.54 | 27 | SiC |
| After Heating | 35.65 | 2.51 | 250 | SiC |
| | 60.00 | 1.54 | 94 | SiC |
| | 71.95 | 1.31 | 78 | SiC |
| | 25.75 | 3.46 | 35 | ? |
| | 41.50 | 2.17 | 30 | SiC |
| | 26.25 | 3.39 | 28 | ? |

to degrade as excess CO evaporated, and β-SiC recrystallized as relatively coarse grains on the rims of the fibers. XRD analysis revealed that the (111) β-SiC peak (d = 2.51A) sharpened and intensified after heat treatment of the fibers. This was attributed to the increase in grain size of the β-SiC. It is reasonable to assume the same expanation here for the sharpening and intensification of SiC peaks. However, some amorphous to crystalline transformation in the matrix and/or fibers may have contributed to the overall increases in intensity and sharpness of the peaks.

The increases in thermal diffusivity upon heating may be due to a variety of factors. First, the chemistry and microstructure of the fibers has been shown to change with heat treatment (30). Initially, the SiC fibers are composed of very fine, polycrystalline β-SiC grains in a matrix of residual carbon, with oxygen and nitrogen impurities. With heating above ≅1200°C, oxygen, nitrogen and carbon impurities were driven off, and the β-SiC recrystallized as larger grains on the rims of the fibers. Increases in grain size only affect thermal diffusivity at temperatures lower than those examined in this study, but devolatization and removal of impurities in the SiC fibers would increase thermal diffusivity, parallel to the fiber plane. Increases in thermal diffusivity (obtained upon heating) perpendicular to the fiber plane result from chemical or microstructural changes in the fibers or in the matrix.

The results, in summary, are as follows:

1. Examination of fibers before and after heating to 1800°C revealed marked differences in their appearance and behavior. This supports the idea that some

compositional or structural change in the fibers themselves is at least one of the sources of annealing effects.

2. Comparison of the diffraction patterns for both low and high char samples before and after heating to 1800°C showed dramatic increases in intensity and sharpness of the SiC peaks. This is probably due to recrystallization of β-SiC on the rims of the fibers.

3. Reflected light microscopy, BSE imagery, and elemental mapping revealed distinct differences between the matricies of the high and low char samples. In the low char samples, SiC was a major, evenly distributed component of the matrix. In contrast, SiC was a minor, unevenly distributed component of the matrix of high char samples. In these samples char predominated as the matrix phase.

4. In equivalent samples, thermal diffusivity parallel to a set of fibers was always higher than thermal diffusivity perpendicular to the crossweave, as expected from general composite theory.

5. Prior to any annealing and parallel to the fibers, thermal diffusivity in all low char samples tested was higher than in the high char samples. Values perpendicular to the fiber plane were roughly the same.

6. In measurements to 1000°C, no samples showed hysteresis effects. Thermal diffusivity tended to increase at the higher temperatures, due to apparent radiation effects.

7. In measurements to 1400°C, the high char samples increased in thermal diffusivity above about 600°C. In the high char sample parallel to one set of fibers, this increase was maintained on cooling.

8. In measurements to 1800°C, all samples showed significant permanent increases in thermal diffusivity. Room temperature diffusivity roughly doubled or trebled. Annealing effects were more pronounced parallel to the fibers, and in the high char samples.

In this study, it was seen that: 1. thermal diffusivity was highest parallel to one set of fibers 2. above 1000°C permanent increases in thermal diffusivity and possibly changes in the mechanical properties may occur 3. the matrix of the high char samples is dominated by char, because the initial presence of phenolic resin inhibited the chemical vapor deposition of SiC. While the first result allows the relative adjustment of thermal diffusivity, the second and third represent warnings and limitations on the application of these materials. Prediction of the behavior of these materials at high temperatures must rely on characterization of the changes that occur in the resin, the fibers, and in the SiC matrix.

Analysis of the behavior and responses of the SiC-SiC composite is a much more complex problem than is the prediction of the behavior of the SiC-Mullite composite material. In the latter, differences in heat conduction behavior could be explained with regard to the expected and common variables of temperature, orientation, and volume percent and type of dispersions in the composite. Analysis of the SiC-SiC system requires the additional consideration of time-temperature effects, the influence of the addition of a third phase to the composite, and consideration of interface effects in light of the presence of the char between the SiC fibers and matrix.

# Recommendations for Future Work

In the SiC-mullite study, only one sample of the VLS whisker reinforced-mullite was available for testing: the 30 w/o SiC-mullite sample. While it is likely that 10 and 20 w/o VLS SiC-mullite samples would display thermal diffusivity values that are higher than the thermal diffusivity of the 10 and 20 w/o RH SiC-mullite samples, verification of this could come from a study of the thermal diffusivity of 10 and 20 w/o VLS SiC whisker-reinforced mullite samples. For good comparison, it is suggested that all of the samples that were prepared for such a testing scheme contain a matrix drawn from the same batch of mullite. Also, the experimental data point for the VLS whisker-reinforced mullite sample plots above the $\frac{K_d}{K_m}$ theoretical curve $= \infty$ (Figure 5), in an imprecise area. A distinct estimate of the thermal conductivity and diffusivity of the VLS whiskers could come from the preparation and examination of a different composite, with a matrix closer in thermal conductivity to the VLS SiC whiskers than is the mullite matrix.

In the SiC-SiC study, better chemical characterization of the char is needed, before and after heating of the char. Also, there is potential for a study of the time-temperature effects on annealing of the SiC-SiC composites. This would require careful control of processing, time, and temperature variables, and extensive pre- and post-heating testing to adequately analyze alterations in the materials due to annealing. In addition, it would be interesting to see if the room temperature thermal diffusivity of low and high char samples manufactured from the same batch of SiC fibers is the same, parallel to one set of fibers.

# Bibliography

1. W. D. Kingery, H. K. Bowen, and D. R. Uhlmann, Introduction to Ceramics, 2nd Edition, 1976, New York, John Wiley & Sons, Inc.

2. K. Schroder, Electronic, Magnetic, and Thermal Properties of Solid Materials, 1978, New York, Marcel Dekker, Inc.

3. D. D. Pollock, Physical Properties of Materials for Engineers, Volume I, 1982, Boca Raton, Florida, CRC Press, Inc.

4. A. E. Powers, "Conductivity in Aggregates," Knolls Atomic Power Laboratory Report, KAPL-2145 (1961).

5. J. J. Brennan, L. D. Bentsen, D. P. H. Hasselman, "Determination of the Thermal Conductivity and Diffusivity of Thin Fibers by the Composite Method," J. Mat. Sc., 17, 2337-42 (1982).

6. H. Tawil, Larry D. Bentsen, S. Baskaran and D. P. H. Hasselman, "Thermal Diffusivity of Chemically Vapor Deposited Silicon Carbide Reinforced with Silicon Carbide or Carbon Fibers," J. Mat. Sc., 20, 3201-12 (1985).

7. D. P. H. Hasselman, L. F. Johnson, R. Syed, Mark P. Taylor, K. Chyung, "Heat Conduction Characteristics of Carbon Fiber Reinforced Lithia-Alumino-Silicate Glass-Ceramic," J. Mat. Sci. (in press).

8. L. F. Johnson, D. P. H. Hasselman, E. Minford, "Thermal Diffusivity and Conductivity of a Carbon Fiber-Reinforced Borosilicate Glass," J. Mat. Sci. (in press).

9. Lloyd F. Johnson, D. P. H. Hasselman, Kenneth Chyung, "Effect of Silicon Carbide Fiber- or Whisker-Reinforcement on the Thermal Diffusivity/Conductivity of an Osmullite Glass-Ceramic," J. Amer. Ceram. Soc. (in press).

10. D. P. H. Hasselman, L. F. Johnson, "Effective Thermal Conductivity of Composites with Interfacial Thermal Barrier Resistance," J. Comp. Materials (in press).

11. Lord Rayleigh, "On the Influence of Obstacles Arranged in Rectangular Order Upon the Properties of a Medium," Phil. Mag. 34, 481-507 (1892).

12. J. C. Maxwell, p. 440 in A Treatise on Electrictiy and Magnetism, 1, 3rd Ed., 1904, Oxford, Oxford University Press.

13. W. D. Kingery, in Progress in Ceramic Science, Volume 2, "The Thermal Conductivity of Ceramic Dielectrics," 1962, New York, Pergamon Press.

14. W. J. Parker, R. J. Jenkins C. P. Butler, G. L. Abbott, "Flash Method of Determining Thermal Diffusivity, Heat Capacity and Thermal Conductivity, " J. Appl. Phys., 32(9) 1679-84 (1961).

15. R. C. Heckman, "Finite Pulse-Time and Heat Loss Effects in Pulse Thermal Diffusivity Measurements," J. Appl. Phys., 44(4) 1455-60 (1973).

16. J. A. Koski, in Thermal Conductivity 18, "Improved Data Reduction Methods for Laser Pulse Diffusitvity Determination with the Use of Microcomputers," in press, New York, Plenum Press.

17. J. V. Milewski, F. D. Gac, J. J. Petrovic, S. R. Skaggs, "Growth of beta-silicon carbide whiskers by the VLS process," J. Mat. Sci., 20 1160-66 (1985).

18. Robert Ruh, K. S. Mazdiyasni, "Fabrication of Mullite-SiC Whisker and Mullite-PSZ-SiC Whisker Composites," pp. 205-215 in Metal, Carbon and Ceramic Matrix Composites, NASA Conference Publication 2406 (1985).

19. Robert Ruh, K. S. Mazdiyasni and M. G. Mendiratta, "Characterization and Properites of Mullite-PSZ-SiC Whisker Composites," Presented at the Eighth Annual Meeting, The American Ceramic Society, Chicago IL, April 29 (1986).

20. Y. S. Touloukian, R. W. Powell, C. Y. Ho, M. C. Nicolaou, Thermophysical Properties of Matter, Vol. 10, Thermal Diffusivity, 1973, New York, IFI/Plenum.

21. M. Srinivasan, L. D. Bentsen, D. P. H. Hasselman, "Thermal Diffusivity of Silicon Carbide-Silicon Composites," Thermal Conductivity 17, pp. 677-87, Ed. by J. G. Hust, Plenum Press (1983).

22. G. A. Slack, "Thermal Conductivity of Pure and Impure Silicon, Silicon Carbide, and Diamond," J. Appl. Phys. 35(12) 3960-66 (1964).

23. J. F. Lynch, C. G. Ruderev, W. H. Duckworth, Engineering Properties of Selected Ceramic Materials, 1966, Columbus, OH, The American Ceramic Society.

24. Y. S. Touloukian, C. Y. Ho, Thermophysical Properties of Matter, Vol. 2, Thermal Conductivity-Nonmetallic Solids, 1970, New York, IFI/Plenum.

25. S. R. Nutt, "Defects in Silicon Carbide Whiskers," J. Amer. Ceram. Soc. 67(6) 428-31 (1984).

26. D. S. Philips, Los Alamos National Lab., Private Communication (1986).

27. Y. S. Touloukian, E. H. Buyco, Thermophysical Properties of Matter Vol. 5, Specific Heat, Nonmetallic Solids, 1970, New York, IFI/Plenum.

28. Lloyd F. Johnson, D. P. H. Hasselman, J. F. Rhodes, (in preparation).

29. B. D. Cullity, Elements of X-ray Diffraction, 2nd Edition, 1978, Reading, Massachusetts, Addison-Wesley Publishing Company.

30. T. Mah, N. L. Hecht, D. E. McCullum, J. R. Hoenigman, H. M. Kim, A. P. Katz, and H. A. Lipsitt, "Thermal Stability of SiC Fibres (NICALON)," J. Mat. Sci. 19, 1191-1201 (1984).

31. M. A. Herron and S. H. Risbud, "Characterization of SiC-Fiber- Reinforced Ba-Si-Al-O-N Glass Ceramic Composites," ACS Bull. 65(2), 342-346 (1986).

32. R. T. Holm, P. H. Klein, and P. E. R. Nordquist, Jr., "Infrared Reflectance Evaluation of Chemically Vapor Deposited β-SiC Films Grown on Si Substrates," J. Appl. Phys. 60(4), 1479-1485 (1986).

33. S. Nishino, Y. Hazuki, H. Matsunami, and T. Tanaka, "Chemical Vapor Deposition of Single Crystalline β-SiC Films on Silicon Substrate with Sputtered SiC Intermediate Layer," J. Electrochem. Soc. 127(12), 2674-2680 (1980).

34. J. J. Petrovic, J. V. Milewski, D. L. Rohr, and F. D. Gac, "Tensile Mechanical Properties of SiC Whiskers," J. Mat. Sci. 20, 1167-1178 (1985).

The vita has been removed from the scanned document